The role of surface stress in structural transitions, epitaxial growth and magnetism on the

nanoscale

The role of surface stress in structural transitions, epitaxial growth and magnetism on the nanoscale

Dirk Sander, Zhen Tian and Jürgen Kirschner

Max Planck Institute of Microstructure Physics, Weinberg 2, 06120 Halle, Germany

E-mail: sander@mpi-halle.de

Abstract
We review results on combined stress measurements by the crystal curvature technique and structural investigations on different nanoscale systems. It is shown that stress measurements offer highly sensitive and accurate data which identify even subtle structural changes in the sub-monolayer coverage regime. We discuss the unique potential of stress measurements to complement structural investigations of atomic layers and at surfaces. Our examples reveal that stress measurements enhance, support and clarify the interpretation of quantitative structural data. The role of surface stress and film stress for structural transitions in epitaxial growth, surfactant-mediated growth, surface reconstruction and adsorbate-induced spin reorientation transitions in monolayers is discussed.

(Some figures in this article are in colour only in the electronic version)

1. Introduction

The progress of quantitative structural analysis by diffraction techniques has led to an accuracy for the positions of atoms at surfaces and in epitaxial layers of the order of picometers (pm), i.e. atomic positions can be reliably experimentally determined on a 0.01 Å scale [1–3]. This is a most remarkable result, as it opens the way to study the impact of even subtle structural changes on the pm scale on other physical properties such as stress and magnetism [4, 5].

Here we present selected results on combined structural and stress measurements. Our examples indicate that stress measurements identify structural changes in atomic layers and at surfaces with high sensitivity. We select results on Ir(100) and Cu(100) surfaces to honor Klaus Heinz and his group, who investigated both surfaces intensively by low energy electron diffraction (LEED) and scanning tunneling microscopy (STM) [6–10].

In the following we present examples of combined stress and diffraction experiments which illustrate clearly that both experimental techniques supplement each other, producing a quantitative understanding of stress–strain relations at surfaces and in epitaxial layers. Our data indicate that continuum elasticity is appropriate to describe both film stress and vertical layer relaxation within the bulk of films thicker than two atomic layers. Our work on surfaces and thinner films points to the importance of surface stress effects and surface relaxation.

The first example below identifies a stress signature of a possible fcc to bcc transition in two to three layer thin epitaxial films of Fe on Ir(100) [4]. Next, we present a stress analysis of surfactant growth of Ni on Cu(100) [11, 12], where our stress data suggest subtle differences in the film structure of an oxygen-mediated surfactant-grown film as compared to film growth without surfactant. The resulting subtle changes of the film structure, which we quantified by surface x-ray diffraction, are expected to have considerable impact on the magnetic properties of the Ni monolayers. This assertion is supported by our third example, a combined stress and LEED analysis of the spin reorientation transition (SRT) of Ni monolayers on Cu(100) [13]. We demonstrate that just a few percent of a layer coverage of hydrogen drive an in-plane to out-of-plane SRT of that system. We conclude our examples with an outlook of combined stress and LEED measurements on the hydrogen-induced change of surface reconstruction of Ir(100)-5 × 1-hex to 5 × 1-H [14]. We discuss how stress measurements may offer a way to investigate the role of surface stress for surface reconstruction.
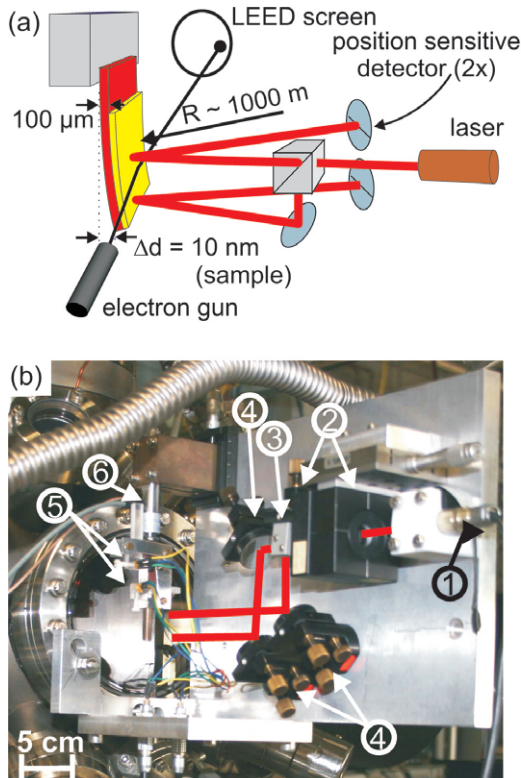
Figure 1. (a) Sketch of the crystal curvature set-up, which we use in Halle to measure stress. The stress-induced curvature of a thin substrate is measured by reflecting two laser beams onto position sensitive detectors. A medium energy electron gun is also available, which we use for *in situ* film thickness calibration by monitoring intensity oscillations on the LEED screen (MEED oscillations; see figure 3). (b) Photograph of the optical components of the set-up. 1, laser; 2, focusing optics; 3, beam splitter; 4, mirror; 5, position sensitive detector (split photodiode); 6, piezo-drive for calibrating the position signal.

2. Stress measurements by the crystal curvature technique

A detailed description and discussion of the crystal curvature technique for stress measurements can be found in numerous review articles [5, 15–21] and books [22–24]. In short, we monitor the stress-induced change of curvature of a rectangular (12 mm long, 2.5 mm wide), thin (0.1 mm) single crystal substrate with an optical laser beam deflection technique. A schematic diagram of the set-up is shown in figure 1. The change of curvature $\Delta(1/R)$ is related to the surface stress change $\Delta\tau = Yt^2/(6(1-\nu))\Delta(1/R)$ (Y, Young's modulus of the substrate; ν, Poisson's ratio of the substrate; t, thickness of the substrate; R, radius of curvature).

The effect of substrate clamping onto the curvature and the elastic anisotropy need to be considered to ensure a reliable quantitative extraction of stress from curvature measurements. A sufficiently large length-to-width ratio of the crystal of at least two to three ensures that the influence of clamping along the width remains negligible, provided the crystal curvature is measured at the lower end [25]. The elastic stiffness of the crystal enters the data evaluation via Young's modulus and

Poisson's ratio, and both quantities need to be calculated for the chosen crystalline orientation of the substrate [16, 21, 26].

Note that $\Delta\tau$ describes a change of surface stress as it occurs, e.g. for a change of the adsorbate coverage. Its unit is N m^{-1}. Another source of stress is the film stress τ_F, which results from the lattice misfit η of an epitaxial film. Its unit is Pa (N m^{-2}), and its magnitude is typically of the order of a few GPa for $\eta = 1\%$. A film stress τ_F induces a curvature change which increases with film thickness t_F, and the following relation holds: $\Delta\tau = \Delta(\tau_F t_F) = Yt^2/(6(1-\nu))\Delta(1/R)$. Thus, the slope of a plot displaying surface stress τ as a function of film thickness t_F gives the film stress τ_F.

The optical crystal curvature detection scheme is sufficiently sensitive to detect the change of surface stress due to a change of adsorbate coverage of less than one per cent of a monolayer. An order of magnitude for the surface stress change of a monolayer coverage is 1 N m^{-1}, and we obtain easily a stress sensitivity better than 0.01 N m^{-1}, as will be demonstrated below for H-induced surface stress on Ni monolayers. A small surface stress change of this magnitude induces a minute deflection of the lower end of the crystal of roughly 0.1 nm, which is straightforwardly detected by the optical deflection technique.

The high sensitivity of the curvature measurement is also used successfully to measure magnetoelastic stress and to perform torque magnetometry with monolayer sensitivity, and the reader is referred to the references for further details [16, 20, 21, 27].

3. Stress signature of a possible fcc to bcc transition in Fe monolayers

The growth of epitaxial Fe layers has attracted a lot of attention as various magnetic phases of Fe have been reported, where a transition between them is driven by structural changes [28–31]. A most interesting aspect is the difference of the magnetic properties of fcc Fe as compared to bcc Fe. A structural distinction between fcc and bcc Fe requires an Fe film thickness in excess of three layers. In thinner films, such a distinction appears to be questionable in view of crystallography [4].

Nevertheless, we propose that a distinction between fcc and bcc is still reasonable and possible, based on other properties of the Fe films, which change with a transition from fcc to bcc. An important example is film stress. Fcc Fe and bcc Fe have different in-plane atomic spacings ($a_{fcc-Fe} = 2.527$ Å, $a_{bcc-Fe} = 2.866$ Å [4]), and consequently the epitaxial growth of each structure gives rise to a different film strain. We calculate a misfit on Ir(100) of $+7.4\%$ and -5.3% for fcc and bcc Fe, respectively. Thus, a measurement of film stress offers a way to discriminate between both modifications, where the fcc phase is correlated with tensile stress, whereas the bcc phase leads to compressive stress [4].

Figure 2 presents a measurement of film stress during the growth of Fe on Ir(100) at 300 K. The stress curve has a negative slope for the deposition of up to 0.5 ML, then a positive slope is observed up to 2 ML, then the slope changes
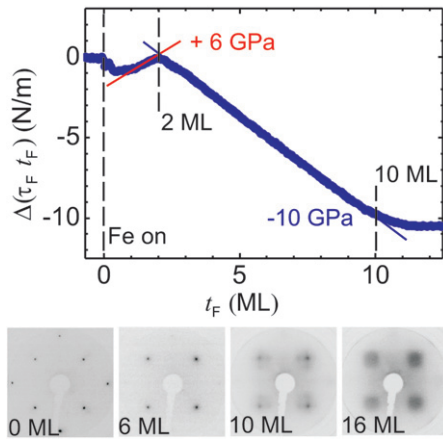
Figure 2. Stress measurement (top) and LEED images at 100 eV (bottom) for the deposition of Fe on Ir(100)-1 × 1 at 300 K. The kink of the stress curve at 2 ML indicates a transition from tensile stress (slope: +6 GPa) to compressive stress (slope: −10 GPa). The stress levels off around 10 ML. The 1 × 1-LEED image at 6 ML indicates pseudomorphic growth; at 10 ML additional diffuse intensity appears around the formerly sharp diffraction pattern, indicative of the end of pseudomorphic growth around 10 ML.

with a sharp kink to a negative value up to the deposition of 10–11 ML, where the slope levels off.

The lower panels show LEED patterns taken at 0, 6, 10 and 16 ML. The patterns show a square symmetry, which indicates epitaxial growth of Fe on Ir(100). The sharp diffraction spots of the LEED pattern of 6 ML, which is very similar to that of clean Ir(100) (0 ML), indicates pseudomorphic growth. Broad intensity distributions around the sharp spots develop around 10 ML and are more pronounced at 16 ML. They indicate the formation of a misfit distortion network starting around 10 ML.

The qualitative inspection of the LEED pattern suggests pseudomorphic growth of Fe on Ir(100) from 0 to 10 ML. This judgment is supported by a detailed quantitative LEED analysis. At higher film thickness, misfit dislocations are formed, and the film is no longer pseudomorphically strained. For the growth of Fe on W(110), pseudomorphic growth ends already in the second layer, and a periodic misfit distortion network is observed in thicker films by surface x-ray diffraction (SXRD) and LEED. Here, a sizeable in-plane lattice strain of +1.2% remains even in 13 ML thick films [32]. Our quantitative structure analysis by SXRD identifies a well ordered two-dimensional array of misfit dislocations with a periodicity of 3.584 and 5.076 nm along the [001] and [$\bar{1}$10] directions, respectively. The relaxation of misfit strain, which amounts to +9.4 % for pseudomorphic growth of Fe on W, is proposed to be the driving force for the formation of this misfit dislocation structure [32].

The initial stress change of up to 0.5 ML Fe deposition is ascribed to a compressive surface stress change due to the adsorption of Fe on clean Ir. Such a compressive surface stress change has been measured before for the growth of 3d metals on W [16, 33] and Ir substrates [14]. It is ascribed to the reduction of the tensile surface stress of the clean substrate upon adsorption of sub-monolayer quantities of other elements [15].

At larger coverage above 0.5 ML the epitaxial misfit of the growing film determines the stress behavior. We observe that the epitaxial misfit stress, as indicated by the slope of the curve, is tensile up to 2 ML, and it changes its sign, indicating compressive stress, at larger thickness. The slope corresponds to a misfit induced stress of +6 GPa and −10 GPa in both regimes, respectively.

We ascribe this change of sign of film stress around 2 ML to the formation of an fcc-Fe precursor up to 2 ML, and to the growth of bcc Fe on top of the precursor for deposition above 2 ML [4]. We conclude that the fcc phase of Fe is the appropriate reference state up to 2 ML, whereas it is the bcc phase in thicker films. For the bcc phase we calculate a misfit stress of −11 GPa, in good quantitative agreement with the measurement. The calculated stress of the fcc phase is +11 GPa. It is of the same sign as in the experiment, but of different magnitude, suggesting that a 2 ML thin Fe film has not developed yet the elastic properties of the reference state.

In LEED, the proposition of a possible Fe fcc precursor is mainly based on the change of layer spacings in thinner films as compared to thicker films. Our stress results support this view strongly by revealing the change of sign of film stress, which results straightforwardly from a transition from fcc to bcc Fe.

4. New insight into surfactant growth: evidence for surfactants also in sub-surface sites

Surfactants have been used to improve the layer-by-layer growth of films, where it has been assumed that the surfactant resides on top of the growing film, not influencing the volume of the growing film [34–38]. However, whether all surfactant atoms do reside on top of the film after termination of growth has not been conclusively studied before. Our combined stress and surface x-ray diffraction experiments indicate that this is not the case. Rather, our results suggest that the surfactant action needs to be ascribed to a surfactant enriched zone which extends over two layers near the surface of the film [11].

We investigate the use of oxygen as a surfactant for the growth of Ni monolayers on Cu(100). A pre-coverage of the Cu(100) surface with oxygen prior to Ni deposition leads to an improved layer-by-layer growth [39, 40]. Here, a pre-coverage of 0.5 ML oxygen at 500 K induces a missing row (MR) reconstruction of Cu(100) onto which the Ni is subsequently deposited at 300 K. This procedure has been proposed to result in a flat Ni film, covered by a c-2 × 2 O structure.

Indeed, our MEED data of figure 3(a) show more intensity oscillations for surfactant growth as compared to non-surfactant growth. This indicates that an improved layer-by-layer growth is achieved. However, our stress measurements reveal important differences of both preparations. The stress measurements of figure 3(b) show a tensile stress of +5.1 N m^{-1} after deposition of 8 ML Ni. This stress is in agreement with the calculated misfit induced film stress for pseudomorphically strained Ni monolayers on Cu(100). The stress measurements for surfactant growth lead to a smaller stress change of +4.6 N m^{-1}.

To compare this value to the stress change measured for non-surfactant growth, we need to consider that after
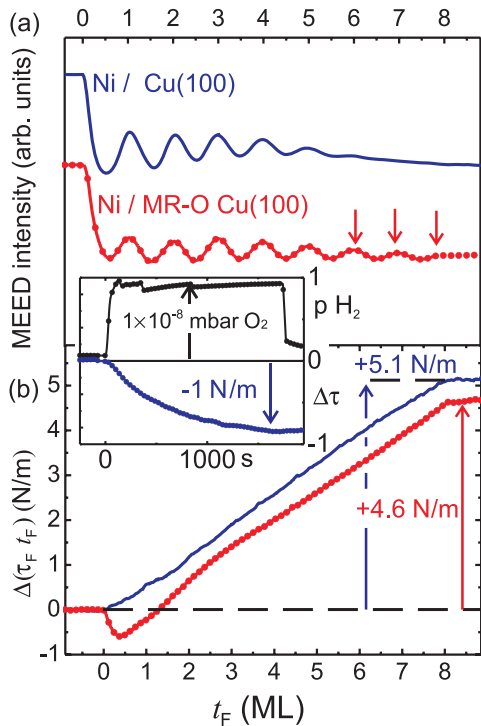
Figure 3. (a) MEED intensity oscillations during the growth of Ni on Cu(100) (upper curve) and on the O-induced missing row (MR) reconstructed Cu(100) (lower curve). More oscillations are observed in the latter case (arrows). (b) Stress measurements for the growth on clean Cu(100) (upper curve, line) and for the O-surfactant growth on MR-O-Cu(100) (lower curve, filled circle). The stress after deposition of 8 ML Ni differs; it is +5.1 N m^{-1} and +4.6 N m^{-1}, respectively. The inset shows a compressive stress change of -1 N m^{-1} for the formation of a c-2 × 2-O structure on 8 ML Ni.

termination of surfactant growth an oxygen coverage of 0.5 is expected at the film surface. Thus, we measure the oxygen-induced stress change of the clean 8 ML Ni film due to the adsorption of a c-2 × 2 O structure with an O coverage of 0.5. We obtain -1 N m^{-1}, as indicated in the inset of figure 3. Thus, the overall stress change for non-surfactant growth with subsequent O adsorption leads to a stress change of +4.1 N m^{-1}. This value differs from +4.6 N m^{-1}, which we measure for surfactant growth. Already from this stress analysis we can draw the important conclusion that both preparations lead to different stresses, and the assumption of a similar structure of both preparations is challenged.

Our detailed surface x-ray diffraction analysis reveals a shortcoming of the simplistic model, which assumes that the surfactant oxygen resides on top of the film. The important new aspect of our structure analysis is that 30% of oxygen resides in sub-surface sites. The structural analysis reveals also significant rumpling and local strain variations near the embedded oxygen atoms. This may influence the surface diffusion of Ni significantly and might be a key for the understanding of the physical origin of surfactant action [11].

These details of the atomic structure of a surfactant-grown film are also decisive for the modified magnetic properties of the oxygen-mediated Ni growth as compared to clean Ni films. The latter shows a spin reorientation transition (SRT) from in

plane to out of plane with *increasing* film thickness at 12 ML Ni, whereas the former shows this SRT already at 5 ML [37]. The magnetic anisotropy of this system depends sensitively on tiny structural changes, as will be demonstrated in the next section, and therefore our new insight into surfactant modified growth also influences the understanding of the magnetic anisotropy of Ni on Cu(100).

5. H-induced surface stress change and spin reorientation transition in Ni monolayers

Ni monolayers on Cu(100) show a peculiar magnetic behavior [41]. The easy magnetization direction is in plane from 0 to 12 ML Ni thickness. For thicker films it reorients to out of plane until the easy magnetization direction reverts back to in plane around 50 ML [42]. The first reorientation is unusual and it is known as an inverse spin reorientation transition.

This sequence of an in-plane easy magnetization direction, followed by an out-of-plane easy magnetization direction with *increasing* film thickness, is reversed as compared to expectations based on the shape anisotropy. The shape anisotropy drives the SRT from out of plane to in plane at a thickness of around 50 ML Ni. It is due to the increasing magnetic stray field energy, which is canceled for an in-plane magnetization direction. But the transition to an out-of-plane magnetization around 12 ML comes as a surprise as also no structural changes are observed in the Ni film at this thickness. The Ni film remains pseudomorphically strained up to 18 ML [13].

We show here that the SRT from in plane to out of plane can be reversibly triggered by changing the hydrogen partial pressure around the sample [13]. At low partial pressure the magnetization of a 8 ML Ni film is in plane, and it switches to out of plane with increasing partial pressure. This reversible switching of the magnetization direction is shown in figure 4(a).

What drives this reversible switching of the magnetization direction? Is it a penetration of hydrogen into the bulk of the film, or is it due to H adsorption in surface sites? Our combined stress and LEED measurements conclusively show that the adsorption and desorption of hydrogen in fourfold hollow sites on the Ni surface is responsible for the H-driven reversible SRT.

We plot the time dependence of the H-induced surface stress change in figure 4(b). To model the adsorption–desorption kinetics we use the adsorption isotherm of H on Ni(100) [43]. At 322 K, a change of partial pressure of hydrogen from 9×10^{-10} to 2×10^{-8} mbar is calculated to change the H coverage from 0.07 to 0.28. The timescale on which this change of H coverage occurs is identical to the time dependence of the H-induced surface stress change, as indicated by the close agreement between the experimental surface stress data and the calculated H coverage in figure 4(b). From this we conclude that the H-induced surface stress change is proportional to the H coverage in this regime. The dynamics of the process are given by the H-adsorption isotherm, and this speaks in favor of H adsorption in surface sites.
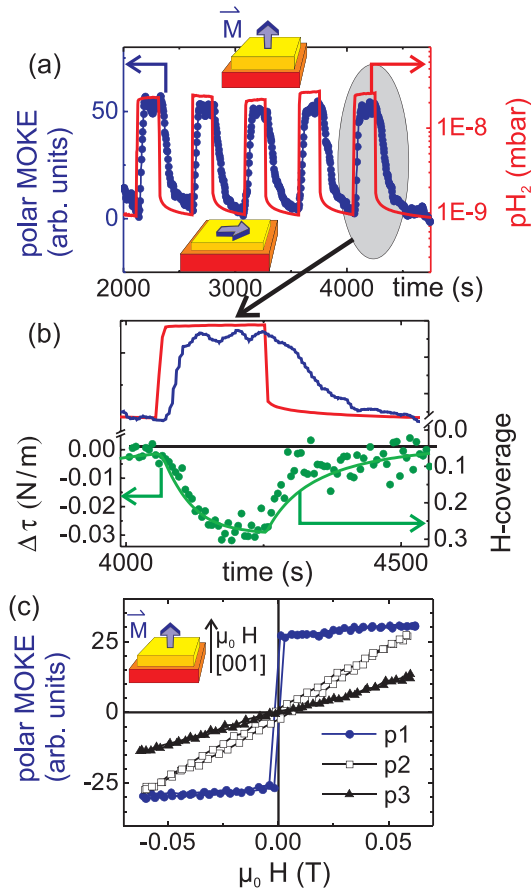
Figure 4. (a) Reversible appearance and decay of the polar magnetization of 8 ML Ni on Cu(100) at 322 K in response to a variation of the H_2 partial pressure. A large partial pressure induces an out-of-plane magnetization direction. A magnetic field of 1 mT is applied normal to the film surface. (b) Zoom-in to the last sequence of (a) with simultaneously taken surface stress measurements (filled circle) and calculated H coverage (solid line through data points). H adsorption can be monitored by the H-induced compressive surface stress change, which changes in proportion to the H surface coverage. (c) Magnetization cycles of 8 ML Ni on Cu(100) measured for different H_2 partial pressures ($p1 = 2.7 \times 10^{-8}$ mbar, $p2 = 1.1 \times 10^{-8}$ mbar, $p3 = 9.3 \times 10^{-10}$ mbar) at 322 K. The curves indicate a transition from a hysteresis-free hard magnetization along the sample normal to an easy polar magnetization for increasing partial pressure.

A quantitative LEED analysis reveals that this H adsorption induces a significant increase of the outermost Ni–Ni layer spacing. Whereas the clean Ni surface has a layer spacing of 1.675 Å, it expands by almost 0.1–1.770 Å upon H adsorption. This effect of H adsorption on the layer spacing is a true surface effect as it decays rapidly in deeper layers [13].

This careful structural analysis opens the way to an understanding of the physical origin of the H-induced SRT of Ni monolayers. The epitaxial misfit between Ni and Cu renders the Ni film in a state of tetragonal distortion. The in-plane strain is $+2.6\%$, the out-of-plane strain is -3.2%. These values are given by the epitaxial misfit between Ni and Cu, and they are confirmed by the LEED analysis [13, 44].

The tetragonal lattice distortion is the driving force for the easy out-of-plane magnetization direction [45–47]. The

atomic distances in plane and out of plane differ; this breaks the cubic symmetry of bulk Ni. The lattice distortion induces a magnetoelastic contribution to the magnetic anisotropy of the film, which favors an out-of-plane easy magnetization direction.

However, figure 4(a) indicates that the clean Ni film does not show an out-of-plane easy magnetization direction. To explain its unexpected in-plane easy magnetization, it has been proposed that in addition to magnetoelastic coupling the surface and interface also contribute to the magnetic anisotropy [41, 45]. Their contributions favor an in-plane easy magnetization direction, which is observed up to 12 ML for the clean film [42].

Thus, our structural analysis suggests that the enlarged layer spacing due to H adsorption reduces the contribution of the surface to the magnetic anisotropy. The layer spacing relaxes by 0.1 Å to 1.770 Å. This layer spacing is very similar to that found in bulk Ni, 1.769 Å. We suggest that this bulk-like layer spacing reduces the magnetic anisotropy of the surface layer, as it renders the film surface in a structure with reduced tetragonal distortion.

In conclusion, our combined surface stress and LEED analysis identifies the adsorption of H in surface sites as the driving force for the H-induced SRT. We ascribe the SRT to the H-induced relaxation of the Ni–Ni layer spacing, and this renders the tetragonal distortion of the *bulk* of the film the decisive contribution to the magnetic anisotropy [16], favoring an out-of-plane easy magnetization direction.

6. Outlook: surface reconstruction in view of combined surface stress and LEED measurements

Numerous surfaces are known to reconstruct [15, 48]. This means that the in-plane atomic arrangements of atoms within the surface plane deviates from that of the layer underneath. Such a surface reconstruction may be induced by thermal treatment of the clean surface layer, or it may be induced by an adsorbate coverage. An example for the former is the herringbone reconstruction of Au(111) [15, 49], and an example for the latter is the C-induced $p4gm$ clock reconstruction of Ni(100) [15, 50]. For these surface reconstructions the change of surface stress upon reconstruction has been measured and the data suggest that the reduction of surface stress is a driving force for these reconstructions [51, 52].

To illustrate handwavingly that surface stress is expected as a possible driving force for surface reconstruction, we note that a surface stress change of 1 N m^{-1}, a magnitude which is typically measured for an adsorbate coverage near unity, corresponds to a significant stress of the surface layer with thickness 1 ML = 2 Å of 5 GPa. The exposure of a elastic material to a stress of this magnitude can indeed produce a sizeable lattice distortion of order several per cent.

A peculiarly transparent relation between surface stress and surface reconstruction has been revealed for the C-induced $p4gm$ reconstruction. Here, both C-induced surface stress [51] and surface phonon dispersion data have been measured [53]. The results suggest a surface-stress-induced softening of a

surface phonon mode as the driving force for this surface reconstruction.

However, in general no clear understanding of the relation between surface stress and surface reconstruction has emerged yet [15, 54]. A most important aspect in this respect is that the surface stress of a clean surface cannot be measured directly. Only the *change* of surface stress upon adsorption and/or reconstruction can be measured. Thus, the magnitude of the surface stress of the unreconstructed surface is not accessible to measurements, and one has to rely on calculations to appreciate whether a large surface stress exists or not [24, 55]. The definition of what magnitude of stress is considered large can be related to the elastic properties of the sample [15].

Calculations suggest that clean metal surfaces have a tensile surface stress [24]. This means that the surface atoms are in a stress state which acts in a direction to bring the atoms closer together. If this tensile stress is large enough, the surface reconstructs and often acquires an atomic arrangement with a higher surface atomic density. This scenario offers a conclusive description of the herringbone reconstruction of Au(111), which has a surface atomic density increased by 4% as compared to Au(111) [15].

Notwithstanding the understanding that a lower total energy of the reconstructed as compared to unreconstructed surface is a mandatory condition for the surface reconstruction to take place, we expect that the magnitude of surface stress should always be lowered upon reconstruction [55]. Thus, measurements of the change of surface stress upon adsorption and reconstruction contribute to a deeper understanding of the driving force behind surface reconstructions.

We show here that the combination of surface stress measurements with LEED intensity measurements allows us to analyze the correlation between surface stress change and structural transition *during* a restructuring process [14]. Thus, not only can the initial and final stage of a structural transition be characterized, but also the time evolution of the transition can be monitored by both surface stress and LEED measurements.

In figure 5 we present stress and LEED data which were taken during the H-induced structural change of the Ir(100)-(5 × 1)-hex to the Ir(100)-(5 × 1)-H surface [7, 8]. As indicated in the sketch of figure 5(a), this transition changes the quasi-hexagonal reconstruction of clean Ir into the 5 × 1-H structure, which is characterized by the arrangements of atomic rows of Ir, separated by five atomic distances on Ir(100).

The increase of the hydrogen partial pressure to 2×10^{-8} mbar leads to a compressive surface stress change, which levels off at -1.7 N m^{-1} after an exposure of several Langmuir, as shown in figure 5(c) (1 L, 1 Langmuir: 1×10^{-6} Torr s). The corresponding structural transition is apparent in the change of the LEED intensity of fractional order and integer order diffraction peaks, shown in figure 5(d). The formation of the 5 × 1-H structure leads to an intensity increase of the integer spots, whereas the fractional order spot decreases in intensity [7].

The measurement of a compressive surface stress change upon lifting of the 5 × 1-hex reconstruction comes as a surprise. One might have expected that the formation of the 5 × 1-hex
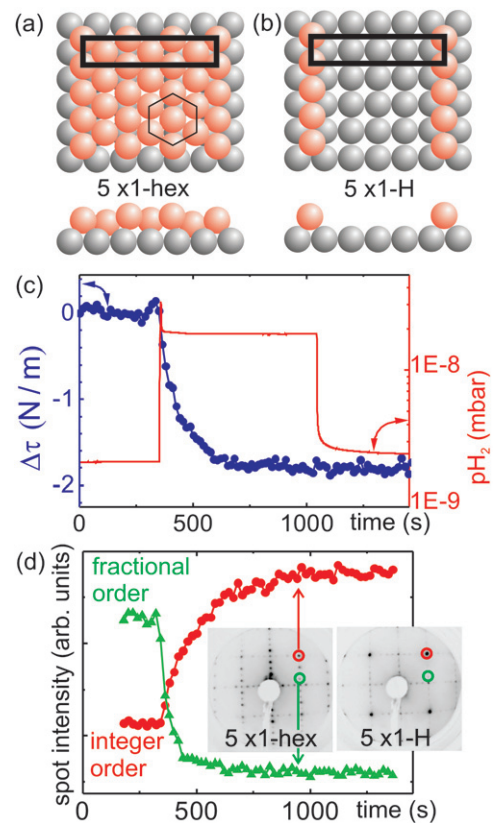

Figure 5. Hard sphere model of the change of surface reconstruction of Ir(100) from (a) 5 × 1-hex to (b) 5 × 1-H, which is triggered by the adsorption of H$_2$ on the quasi-hexagonal reconstructed surface at 300 K. (c) The surface stress change upon this H-induced change of surface reconstruction is -1.7 N m^{-1}. (d) LEED intensity measurements of the integer and fractional order spots, taken under the same experimental conditions as in (c), indicate an increase of intensity of the former, and a decrease of intensity of the latter upon the H-induced change of the surface reconstruction. These diffraction spots are circled in the LEED images (180 eV) shown as the inset, where already a qualitative inspection reveals an increased intensity of the integer order spot upon change of reconstruction.

reconstruction is driven by the large tensile surface stress of the unreconstructed Ir(100) surface. Calculations of surface stress of Ir(100), however, give a non-conclusive picture [56]. The surface reconstruction leads to a very dense surface layer of the 5 × 1-hex phase, which has an atomic surface density increased by 20% as compared to the 1 × 1-phase of Ir(100). Tentatively, this higher surface atomic density could be correlated with compressive surface stress. In order to explain the measured compressive surface stress change, one would have to postulate that H adsorption leads to an even larger compressive surface stress as compared to the 5 × 1-hex phase.

However, in view of the structural model of figure 5(b) this proposition is most remarkable, as at least some fraction of the 5×1-H phase in between the Ir rows displays the characteristics of the 1 × 1-phase of Ir(100). This phase, however, is expected to show a tensile surface stress. Therefore, the notion of an overall compressive surface stress, larger in magnitude than the postulated compressive surface stress of the 5 × 1-hex phase, appears to be surprising.

We may speculate that the structural relaxation of the atomic positions of the 5 × 1-H phase, which has been identified by LEED [7], may play a crucial role for the resulting surface stress. These relaxations could induce a repulsive elastic inter-row interaction, which would also stabilize the parallel arrangement of Ir rows, as observed in experiments [7]. However, currently our understanding of the correlation between structural surface relaxations and surface stress is rather incomplete [57], and no quantitative assessment can be given.

We conclude with the remark that the line of thought of the last two paragraphs is highly speculative. It reflects our lack of knowledge about the absolute value of surface stress, and about its physical origin. Here, calculations offer currently the only way to put the discussion of surface stress and its role in surface reconstruction on a solid basis [55]. Our combined stress and structure measurements contribute to a better understanding by offering quantitative reference data for such theoretical studies.

7. Conclusion

Stress measurements by the cantilever curvature technique offer quantitative data on adsorbate-induced surface stress, film stress, and surface stress change upon surface reconstruction. These data elucidate the correlation between stress and structural transitions at surfaces and in atomic layers. Our data suggest that the stress–strain relation in films thicker than 2 ML can often be well described by the respective expression of continuum elasticity. At surfaces, or in films thinner than 2 ML, this description may break down. The origin of stress in the sub-monolayer coverage regime or even of clean surfaces has not been extensively tackled by either experiment or theory so far. It remains a challenging task to identify the impact of minute structural changes on the pm scale on other physical properties such as stress and magnetism. In this respect, the combination of stress and structural investigations offers accurate quantitative data, which may serve as a reference for theoretical work.

References

[1] Heinz K 1988 Structural analysis of surfaces by LEED *Prog. Surf. Sci.* **27** 239–326

[2] Heinz K 1995 LEED and DLEED as modern tools for quantitative surface structure determination *Rep. Prog. Phys.* **58** 637–704

[3] Heinz K 2003 Crystallography of magnetic nanostructures—structural complexity versus accuracy *J. Phys.: Condens. Matter* **15** S655

[4] Martin V, Meyer W, Giovanardi C, Hammer L, Heinz K, Tian Z, Sander D and Kirschner J 2007 Pseudomorphic growth of Fe monolayers on Ir(001)-(1 × 1): from a fct precursor to a bct film *Phys. Rev.* B **76** 205418

[5] Sander D 2004 The magnetic anisotropy and spin reorientation of nanostructures and nanoscale films *J. Phys.: Condens. Matter* **16** R603–36

[6] Heinz K, Müller S and Hammer L 1999 Crystallography of ultrathin iron, cobalt and nickel films grown epitaxially on copper *J. Phys.: Condens. Matter* **11** 9437–54

[7] Hammer L, Meier W, Klein A, Landfried P, Schmidt A and Heinz K 2003 Hydrogen-induced self-organized nanostructuring of the Ir(100) surface *Phys. Rev. Lett.* **91** 156101

[8] Heinz K, Hammer L, Klein A and Schmidt A 2004 Nanowire formation without surface sterps *Appl. Surf. Sci.* **237** 519–27

[9] Heinz K and Hammer L 2004 Combined application of LEED and STM in surface crystallography *J. Phys. Chem.* B **108** 14579–84

[10] Giovanardi C, Hammer L and Heinz K 2006 Ultrathin cobalt oxide films on Ir(100)-(1 × 1) *Phys. Rev.* B **74** 125429

[11] Meyerheim H L, Sander D, Popescu R, Pan W, Popa I and Kirschner J 2007 Surfactant-mediated growth revisited *Phys. Rev. Lett.* **99** 116101

[12] Meyerheim H L, Sander D, Negulyaev N N, Stepanyuk V S, Popescu R, Popa I and Kirschner J 2008 Meyerheim *et al* reply *Phys. Rev. Lett.* **100** 089602

[13] Sander D, Pan W, Ouazi S, Kirschner J, Meyer W, Krause M, Müller S, Hammer L and Heinz K 2004 Reversible H-induced switching of the magnetic easy axis in Ni/Cu(001) thin films *Phys. Rev. Lett.* **93** 247203

[14] Tian Z 2008 Magnetoelastic coupling in ferromagnetic film and surface stress studies on Ir(100) *PhD Thesis* Martin Luther University Halle-Wittenberg

[15] Ibach H 1997 The role of surface stress in reconstruction, epitaxial growth and stabilization of mesoscopic structures *Surf. Sci. Rep.* **29** 193–264

[16] Sander D 1999 The correlation between mechanical stress and magnetic anisotropy in ultrathin films *Rep. Prog. Phys.* **62** 809–58

[17] Sander D 2003 Surface stress: implications and measurements *Curr. Opin. Solid State Mater. Sci.* **1** 51–7

[18] Sander D, Meyerheim H, Ferrer S and Kirschner J 2003 Stress, strain, and magnetic anisotropy: all is different in nanometer thin films *Adv. Solid State Phys.* **43** 547–61

[19] Kury P, Grabosch T and Horn von Hoegen M 2005 SSIOD: the next generation *Rev. Sci. Instrum.* **76** 023903

[20] Sander D and Kirschner J 2007 Cantilever stress measurements of ferromagnetic monolayers *Appl. Phys.* A **87** 419–25

[21] Sander D, Tian Z and Kirschner J 2008 Cantilever measurements of surface stress, surface recconstruction, film stress and magnetoelastic stress of monolayers *Sensors* **8** 4466–86

[22] Koch R 1997 Intrinsic stress of epitaxial thin films and surface layers *The Chemical Physics of Solid Surfaces* vol 8 (Amsterdam: Elsevier)

[23] Hanbücken M and Deville J P (ed) 2001 *Stress and Strain in Epitaxy: Theoretical Concepts, Measurements and Applications* (Amsterdam: Elsevier)

[24] Sander D and Ibach H 2002 *Landolt-Börnstein, Numerical Data and Functional Relationships in Science and Technology, New Series* Group III: Condensed Matter, vol 42, A 2 (Berlin: Springer) chapter 4.4 (Surface Free Energy and Surface Stress) pp 4.4-1–49

[25] Dahmen K, Lehwald S and Ibach H 2000 Bending of crystalline plates under the influence of surface stress *Surf. Sci.* **446** 161–73

[26] Brantley W A 1973 Calculated elastic constants for stress problems associated with semiconductor devices *J. Appl. Phys.* **44** 534–5

[27] Gutjahr-Löser Th, Sander D and Kirschner J 2000 Magnetoelastic coupling in Co thin films on W(001) *J. Magn. Magn. Mater.* **220** L1–7

[28] Moruzzi V L, Marcus P M and Kübler J 1989 Magnetovolume instabilities and ferromagnetism versus antiferromagnetism in bulk fcc iron and manganese *Phys. Rev.* B **39** 6957–61

[29] Thomassen J, May F, Feldmann B, Wuttig M and Ibach H 1992 Magnetic live surface layers in Fe/Cu(100) *Phys. Rev. Lett.* **69** 3831–4

[30] Wuttig M and Liu X 2004 Ultrathin metal films *Springer Tracts in Modern Physics* vol 206 (Berlin: Springer)

[31] Müller S, Bayer P, Reischl C, Heinz K, Feldmann B, Zillgen H and Wuttig M 1995 Structural instability of ferromagnetic fcc Fe films on Cu(100) *Phys. Rev. Lett.* **74** 765–8

[32] Popescu R, Meyerheim H L, Sander D, Kirschner J, Steadman P, Robach O and Ferrer S 2003 Surface x-ray structure analysis of periodic misfit dislocations in Fe/W(110) *Phys. Rev.* B **68** 155421

[33] Meyerheim H L, Sander D, Popescu R, Kirschner J, Robach O, Ferrer S and Steadman P 2003 Ni-induced giant stress and surface relaxation in W(110) *Phys. Rev.* B **67** 155422

[34] Egelhoff W F Jr and Steigerwald D A 1989 The role of adsorbed gases in metal on metal epitaxy *J. Vac. Sci. Technol.* A **7** 2167–73

[35] van der Vegt H A, van Pinxteren H M, Lohmeier M, Vlieg E and Thornton J M C 1992 Surfactant-induced-layer-by-layer growth of Ag on Ag(111) *Phys. Rev. Lett.* **68** 3335–8

[36] Camarero J, Graf T, de Miguel J J, Miranda R, Kuch W, Zharnikov M, Dittschar A, Schneider C M and Kirschner J 1996 Surfactant-mediated modification of the magnetic properties of Co /Cu(111) thin films and superlattices *Phys. Rev. Lett.* **76** 4428–31

[37] Hong J, Wu R Q, Lindner J, Kosubek E and Baberschke K 2004 Manipulation of spin reorientation transition by oxygen surfactant growth: a combined theoretical and experimental approach *Phys. Rev. Lett.* **92** 147202

[38] Sorg C, Ponpandian N, Bernien M, Baberschke K, Wende H and Wu R Q 2006 Induced magnetism of oxygen in surfactant-grown Fe, Co, and Ni monolayers *Phys. Rev.* B **73** 064409

[39] Nünthel R, Gleitsmann T, Poulopoulos P, Scherz A, Lindner J, Kosubek E, Litwinski Ch, Li Z, Wende H, Baberschke K, Solbov S and Rahman T S 2003 Epitaxial growth of Ni on Cu(100) with the assistance of o-surfactant and its magnetism compared to Ni(100)/Cu(100) *Surf. Sci.* **531** 53–67

[40] Lindner J, Poulopoulos P, Nünthel R, Kosubek E, Wende H and Baberschke K 2003 Improved growth and the spin reorientation transition of Ni on sqrt2 times 2sqrt 2 R45 reconstructed O/Cu(100) *Surf. Sci.* **523** L65–9

[41] Schulz B and Baberschke K 1994 Crossover from in-plane to perpendicular magnetization in ultrathin Ni/Cu(001) films *Phys. Rev.* B **50** 13467–71

[42] Vollmer R, Gutjahr-Löser Th, Kirschner J, van Dijken S and Poelsema B 1999 Spin reorientation transition in Ni films on Cu(001): the influence of H_2 adsorption *Phys. Rev.* B **60** 6277–80

[43] Christmann K, Schober O, Ertl G and Neumann M 1974 Adsorption of hydrogen on a nickel single crystal surfaces *J. Chem. Phys.* **60** 4528–40

[44] Platow W, Bovensiepen U, Poulopoulos P, Farle M, Baberschke K, Hammer L, Walter S, Müller S and Heinz K 1999 Structure of ultrathin Ni/Cu(001) films as a function of thickness, temperature, and magnetic order *Phys. Rev.* B **59** 12641–6

[45] Uiberacker C, Zabloudil J, Weinberger P, Szunyogh L and Sommers C 1999 Lattice relaxation driven reorientation transition in Ni_n/Cu(100) *Phys. Rev. Lett.* **82** 1289–92

[46] Maca F, Shick A B, Redinger J, Podloucky R and Weinberger P 2003 The influence of hydrogen adsorption on magnetic properties of Ni/Cu(001) surface *Czech. J. Phys.* **53** 33–9

[47] Maca F, Shick A B, Schneider G and Redinger J 2004 The spin-reorientation transition on Ni/Cu(001) surfcae covered with hydrogen *J. Magn. Magn. Mater.* **2772-276** 1194–5

[48] King D A and Woodruff D P (ed) 1994 *The Chemical Physics of Solid Surfaces* vol 7 *Phase Transitions and Adsorbate Restructuring at Metal Surfaces* (Amsterdam: Elsevier)

[49] Barth J V, Brune H, Ertl G and Behm R J 1990 Scanning tunneling microscopy observations on the reconstructed Au(111) surface: atomic structure, long-range superstructure, rotational domains, and surface defects *Phys. Rev.* B **42** 9307–18

[50] Onuferko J H, Woodruf D P and Holland B W 1979 LEED structure analysis of the Ni100 (2×2)C(p4g) structure: a case of adsorbate-induced substrate distortion *Surf. Sci.* **87** 357–74

[51] Sander D, Linke U and Ibach H 1992 Adsorbate-induced surface stress: sulfur, oxygen and carbon on Ni(100) *Surf. Sci.* **272** 318–25

[52] Bach C E, Giesen M, Ibach H and Einstein T L 1997 Stress relief in reconstruction *Phys. Rev. Lett.* **78** 4225–8

[53] Müller J E, Wuttig M and Ibach H 1986 Adsorbate-induced surface stress: phonon anomaly and reconstruction on Ni(100) surfaces *Phys. Rev. Lett.* **56** 1583–6

[54] Feibelman P J 1997 First-principles calculations of stress induced by gas adsorption on Pt(111) *Phys. Rev.* B **56** 2175–82

[55] Harrison M J, Woodruf D P, Robinson J, Sander D, Pan W and Kirschner J 2006 Adsorbate-induced surface reconstruction and surface stress changes in Cu(100)/O: experiment and theory *Phys. Rev.* B **74** 165402

[56] Ibach H 1999 Erratum to: the role of surface stress in reconstruction, epitaxial growth and stabilization of mesoscopic structures *Surf. Sci. Rep.* **35** 71–3

[57] Sander D, Schmidthals C, Enders A and Kirschner J 1998 Stress and structure of Ni monolayers on W(110): the importance of lattice mismatch *Phys. Rev.* B **57** 1406–9